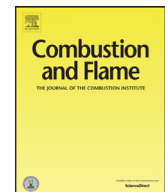




Contents lists available at ScienceDirect

Combustion and Flame

journal homepage: www.elsevier.com/locate/combustflameEffects of radiation reabsorption on laminar NH₃/H₂/air flamesShu Zheng^a, Hao Liu^a, Ran Sui^b, Bo Zhou^c, Qiang Lu^{a,*}^a National Engineering Laboratory for Biomass Power Generation Equipment, North China Electric Power University, Beijing 102206, China^b Department of Mechanical and Aerospace Engineering, Missouri University of Science and Technology, Rolla, MO 65409, USA^c Department of Mechanics and Aerospace Engineering, Southern University of Science and Technology, Shenzhen 518055, PR China

ARTICLE INFO

Article history:

Received 20 May 2021

Revised 13 August 2021

Accepted 16 August 2021

Available online xxx

Keywords:

Radiation reabsorption

Ammonia flame

Flame speed

Elevated pressure

ABSTRACT

Ammonia combustion, owing to its zero greenhouse gas CO₂ emission, is attracting attention for energy utilization. However, the thermal radiation of NH₃ has not been reported and involved in the numerical simulations of ammonia flames, which may cause serious errors in estimating the laminar flame speeds. In this study, the effects of radiation reabsorption on the laminar flame speed at different equivalence ratios and elevated pressures were numerically investigated using planar NH₃/H₂/air flames. The Statistical Narrow-Band (SNB) model parameters for NH₃ were generated and used for simulations of NH₃/H₂/Air flames, considering the radiation reabsorption. It was found that the radiation reabsorption exhibited a non-monotonic behavior at $\phi = 0.65\text{--}1.6$, with the maximum enhancement of flame speed up to 15.6%. The effects of radiation reabsorption were controlled by both radiation and chemistry. The preheat-induced chemical effect dominated at $\phi = 0.65\text{--}1.25$ and the enhancement of flame speed was mainly influenced by H, OH and NH₂ radicals, which were primarily controlled by the reactions R36, R257 and R246, respectively. In contrast, the direct radiation effect dominated at $\phi = 1.25\text{--}1.6$ and the enhancement of flame speed was mainly affected by the increasing mole fraction of NH₃. With increasing pressures, the preheat-induced chemical effect dominated at $P = 1\text{--}10$ atm and the enhancement of flame speed were mainly impacted by H and NHH radicals, which were controlled by the reactions R44 and R257, respectively. At higher pressures above 10 atm, direct radiation effect was dominating and the enhancement of flame speed was mainly controlled by the increasing optical thickness.

© 2021 The Combustion Institute. Published by Elsevier Inc. All rights reserved.

1. Introduction

Ammonia has recently been attracted great attention as a clean and carbon-free fuel. Known as "the other hydrogen", ammonia produces no greenhouse gas CO₂ emissions during its combustion, and hence its usage as a fuel can effectively alleviate the problem of global warming [1]. Moreover, 1 m³ liquid ammonia stores 108 kg hydrogen element at 20 °C and 8.6 atm, which is more than 4 times hydrogen storage capacity of some advanced hydrogen storage alloys [2]. Therefore, the popularization and application of ammonia as a fuel is expected to facilitate the transformation of traditional "carbon-based" energy structure to "hydrogen-based" energy structure.

Several previous studies have attempted to directly burn ammonia in, e.g., engines, boilers and gas turbines [3,4]. However, ammonia has low chemical reactivity and its spontaneous and forced ignitions are relatively difficult compared with traditional hydrocarbon fuels [5,6]. The laminar flame speed of a stoichiometric am-

nia/air mixture is only about 1/5–1/7 of conventional hydrocarbon fuels, and the flame stability is poor [7,8]. To overcome these difficulties, it can be achieved by blending NH₃ with H₂ [9,10], CH₄ [11,12], syngas [13,14] and other hydrocarbon fuels [15].

In terms of experimental research, Lee et al. [16] measured the laminar flame properties of NH₃/H₂/air flames using propagating spherical flames at atmospheric pressure, equivalence ratios 0.6–1.67 and X_{H2} 0–0.5. They found NO_x emission increased less in fuel-rich cases than in fuel-lean cases as X_{H2} increased. Kumar and Meyer [10] studied the laminar flame speeds of NH₃/H₂/air jet flames based on a Bunsen burner at equivalence ratios 0.5–1.1 and X_{NH3} 0–0.8, and compared the predicted laminar flame speeds calculated by the GRI-Mech 3.0 [17], Tian [18] and Konnov [19] chemical kinetic mechanisms. To avoid uncertainties in the measurements of laminar burning velocity caused by the stretch effect on the flame front, Han et al. [11] used the heat flux method to measure the laminar burning velocities of NH₃ blended with H₂, CO and CH₄, and the results were validated by three chemical kinetic mechanisms: GRI-Mech 3.0 [17], Okafor et al. [12] and UC-San Diego [20]. At elevated pressure conditions, Ichikawa et al. [9] experimentally investigated the Markstein

* Corresponding author.

E-mail addresses: qianglu@mail.ustc.edu.cn, qlu@ncepu.edu.cn (Q. Lu).

lengths of $\text{NH}_3/\text{H}_2/\text{air}$ flames at pressures up to 5 atm and numerically simulated the flame characteristics using five different mechanisms. Subsequently, Okafor et al. [21] developed a reduced reaction mechanism and studied the unstretched laminar burning velocity of $\text{NH}_3/\text{CH}_4/\text{air}$ flames at pressures up to 5 atm, equivalence ratios 0.7–1.3 and X_{NH_3} 0–0.3. To investigate the blending effects of syngas in the NH_3 flames, Wang et al. [14] measured the laminar burning velocities of $\text{NH}_3/\text{syngas}/\text{air}$, $\text{NH}_3/\text{CO}/\text{air}$ and $\text{NH}_3/\text{H}_2/\text{air}$ at pressures up to 5 atm, equivalence ratios 0.7–1.6, X_{NH_3} 0.2–1.0 and compared the simulation results of four mechanisms: Han et al. [13], Shrestha et al. [22], UC-San Diego [20] and Stagni et al. [23].

Currently, a few ammonia oxidation mechanisms have been developed to predict the burning velocity of ammonia flames. Miller et al. [24] first proposed a detailed ammonia oxidation mechanism that consists 22 species and 98 reactions. Lindstedt et al. [25] established a comprehensive chemical kinetic mechanism based on abundant experimental data of $\text{NH}_3/\text{H}_2/\text{O}_2/\text{Ar}$, $\text{NH}_3/\text{NO}/\text{H}_2/\text{O}_2/\text{Ar}$ and $\text{NH}_3/\text{O}_2/\text{Ar}$ flames. Skreiber et al. [26] studied the fuel-rich kinetics of ammonia and pointed out that the conversion of fuel-N into N_2 mainly depended on the reaction of NH_2+NO . Recently, Okafor et al. [12] developed a detailed mechanism for $\text{NH}_3/\text{CH}_4/\text{air}$ flames based on GRI-Mech 3.0 [17] and some important reactions from Tian's mechanism [27]. In spite of these previous studies, there are still gaps between the experimental and predictions by mentioned above mechanisms.

To simulate the flame properties accurately, radiative heat transfers should be considered, especially through the loss from the downstream burnt products and reabsorption by the upstream unburned mixture. Previous investigations on radiative heat loss in NH_3/air flames [28] revealed that the laminar flame speed decreased due to the radiative heat loss based on the optically thin model (OTM). It was found that the laminar propagation speed could be reduced by 3% near the stoichiometric condition, while reduction greater than 20% was observed near the flammability limit. For the radiation reabsorption, Ju et al. [29] first studied the radiation reabsorption effects on burning velocities of CH_4/air flames with CO_2 dilution and found the burning velocities increased and the flammability limit was extended due to the reabsorption. Subsequently, Chen et al. [30,31] investigated the radiation reabsorption and compression effects on flame speeds of CH_4/air spherical flames with $\text{CO}_2/\text{CO}/\text{H}_2\text{O}$ dilutions using fitted statistically narrow band correlated k (FSNB-CK) model. Zheng et al. [32] calculated the effects of radiation reabsorption on the burning fluxes of CH_4/air flames with CO_2 addition at high pressures up to 25 atm based on the band lumping model. Generally, all these studies only focused on the effects of radiation reabsorption of CO_2 , H_2O and CO on burning velocities. To the best of our knowledge, there is yet no investigation reported on the effects of radiation reabsorption of NH_3 on the ammonia flames.

The goal of this study is to assess the effects of NH_3 radiation on the laminar flame speed when radiation reabsorption is considered in planar $\text{NH}_3/\text{H}_2/\text{air}$ flames. First, the SNB model for NH_3 was developed and the accuracy was validated by line-by-line (LBL). Subsequently, numerical simulations were conducted for laminar premixed $\text{NH}_3/\text{H}_2/\text{air}$ flames at various equivalence ratios and high pressures with and without including radiation reabsorption. Finally, the chemical and radiation effects of radiation reabsorption on laminar flame speeds were discussed.

2. Numerical model and validation

One-dimensional freely-propagating laminar premixed $\text{NH}_3/\text{H}_2/\text{Air}$ flames were simulated using the PREMIX code [33]. The kinetic modeling and transport properties were evaluated by the CHEMKIN and TRANSPORT packages, and the detailed ammonia reaction mechanism of Okafor et al. [12] was employed.

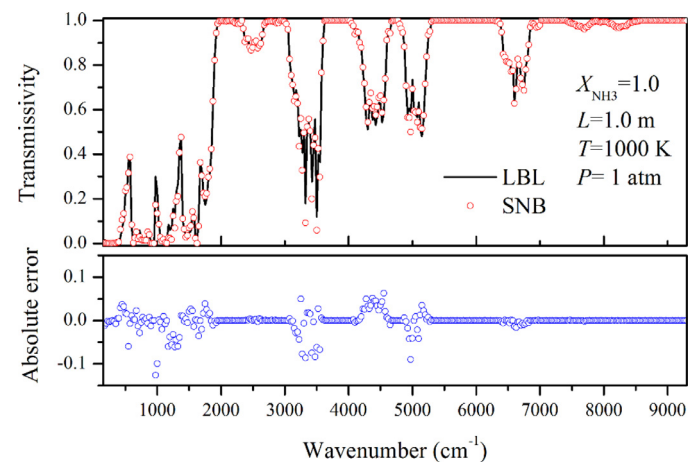


Fig. 1. Comparison of narrow-band transmissivities calculated by SNB and LBL models at $X_{\text{NH}_3} = 1.0$, $L = 1.0 \text{ m}$, $T = 1000 \text{ K}$, $P = 1 \text{ atm}$.

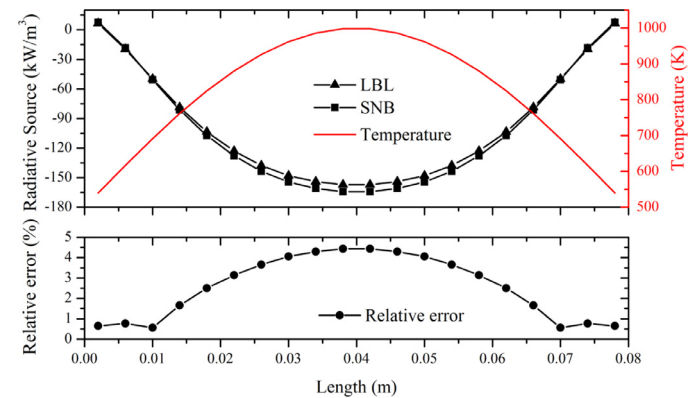


Fig. 2. Comparison of predicted radiative heat source for NH_3 in a one-dimensional parallel-plane layer at $X_{\text{NH}_3} = 1.0$, $L = 0.08 \text{ m}$, $T = 500[1+\sin(\pi x/L)] \text{ K}$, $T_b = 300 \text{ K}$, $P = 1 \text{ atm}$.

To quantify the radiation reabsorption effects, three models were used in the calculation for comparisons: ADI (adiabatic model), OTM (optically thin model) and SNB (statistical narrow-band model).

In the SNB, the narrow band gas transmissivity for path-length L , with gas species mole fraction X and pressure P was evaluated by [34]

$$\bar{\tau}_\eta(L) = \exp \left[-\frac{\pi B}{2} \left(\sqrt{1 + \frac{4SL}{\pi B}} - 1 \right) \right] \quad (1)$$

where $B = 2\bar{\beta}_\eta/\pi^2$, $S = \bar{\kappa}_\eta XP$ and $\bar{\beta}_\eta = 2\pi\bar{\gamma}_\eta/\bar{\delta}_\eta$. The parameters $\bar{\kappa}_\eta$, $\bar{\gamma}_\eta$ and $\bar{\delta}_\eta$ are the narrow band average spectral line strength, the narrow band average spectral line half band-width and the narrow band average spectral line interval, respectively. In this paper, the narrow band parameters for H_2O were taken from Soufiani and Taine [35] based on the EM2C database. The NH_3 mean narrow band parameters were calculated from the HITRAN 2016 database [36], which covers a temperature range of 300 K to 2900 K with a uniform bandwidth of 25 cm⁻¹ between 150 and 9300 cm⁻¹. To validate the SNB parameters of NH_3 , the transmissivities calculated by the SNB and LBL methods were compared and the absolute errors $\bar{\tau}_{\text{SNB},\eta} - \bar{\tau}_{\text{LBL},\eta}$ are shown in Fig. 1. The maximum absolute error was only -0.126 , which appeared at 950 cm⁻¹. This justified that the SNB model of NH_3 could well reproduce the results of LBL.

The SNB model was incorporated into the radiative transfer equation (RTE) in integral form and the ray-tracing method [37,38]

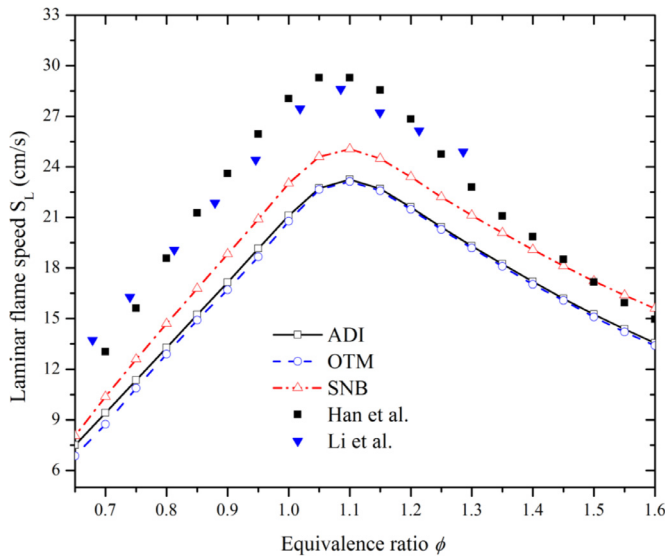


Fig. 3. Laminar flame speed as a function of equivalence ratio ϕ calculated by different radiation models for planar NH_3/H_2 /air flames ($X_{\text{NH}_3}/(X_{\text{NH}_3}+X_{\text{H}_2}) = 0.6$). Black symbols represent experimental data from Han et al. [11], Blue symbols represent experimental data from Li et al. [39].

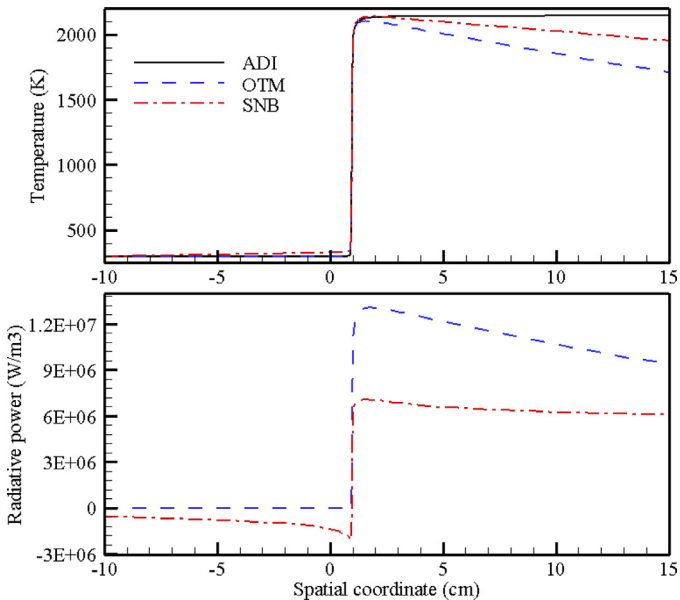


Fig. 4. Distributions of temperature and radiative power in a planar NH_3/H_2 /air flame ($X_{\text{NH}_3}/(X_{\text{NH}_3}+X_{\text{H}_2}) = 0.6$, $\phi = 1.0$).

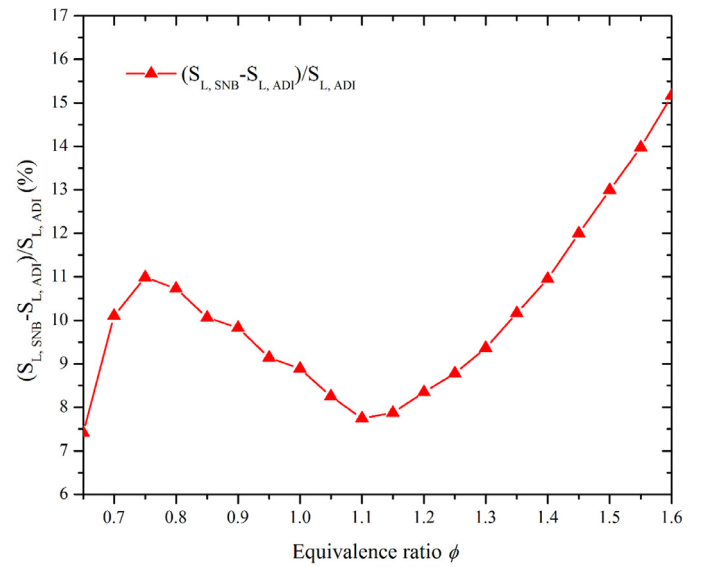
can be used to solve the integral RTE. After getting the radiation intensity, the radiative heat flux and heat source can be obtained by

$$q(x_i) = \sum_{all} \eta \left(\sum_{m=1}^M \xi^m I_{\eta,i}^m w^m \right) \Delta \eta \quad (2)$$

$$\frac{dq}{dx} = -\frac{q_{i+1} - q_i}{x_{i+1} - x_i} \quad (3)$$

where $\Delta \eta$ is 25 cm^{-1} , ξ^m and w^m are the direction cosines and weight function associated with the m th direction, respectively.

To assess the performance of the above radiation model in predicting the radiation heat transfer of NH_3 , we calculated the radiative heat source of NH_3 in a one-dimensional parallel-plane layer as shown in Fig. 2. The thickness of the layer was 0.08 m and the



(a)

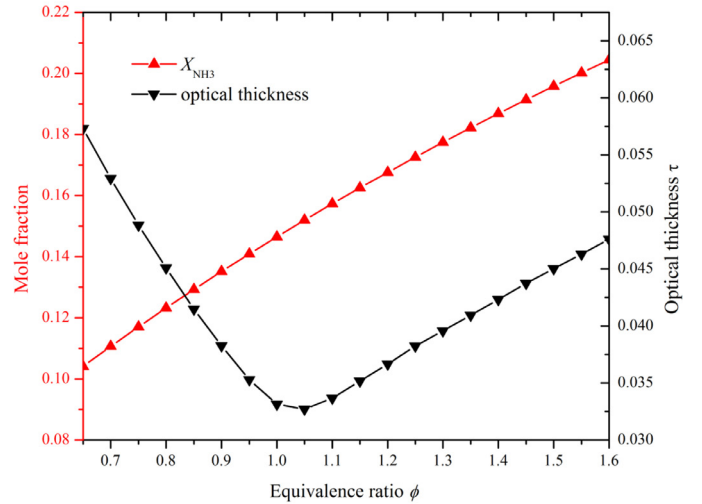


Fig. 5. (a) Radiation absorption effects on the laminar flame speed as a function of ϕ in planar NH_3/H_2 /air flames ($X_{\text{NH}_3}/(X_{\text{NH}_3}+X_{\text{H}_2}) = 0.6$); (b) NH_3 mole fractions in the upstream and optical thickness as a function of ϕ .

temperatures of NH_3 was a sine temperature distribution given as $500[1+\sin(\pi x/L)]$ K. The temperature of the boundary walls was 300 K and non-emitting. As shown in Fig. 2, the relative errors of radiative heat source were less than 4.5%, manifesting very satisfactory predictions by the SNB, which agreed very well with the LBL results.

3. Results and discussion

3.1. Effects of equivalence ratio ϕ

Laminar flame speeds as a function of equivalence ratio ϕ (0.65–1.6) calculated by the different radiation models (ADI, OTM and SNB) for NH_3/H_2 /air mixtures (with a fixed $\text{NH}_3:\text{H}_2$ ratio $X_{\text{NH}_3}/(X_{\text{NH}_3}+X_{\text{H}_2}) = 0.6$) are shown in Fig. 3. Experimental results by Han et al. [11] and Li et al. [39] are included in the figure for comparison, which used adiabatic stretchless flat flames in a specially modified heat flux burner. Fig. 3 shows that the flame speeds calculated by the OTM were lower than those calculated by the

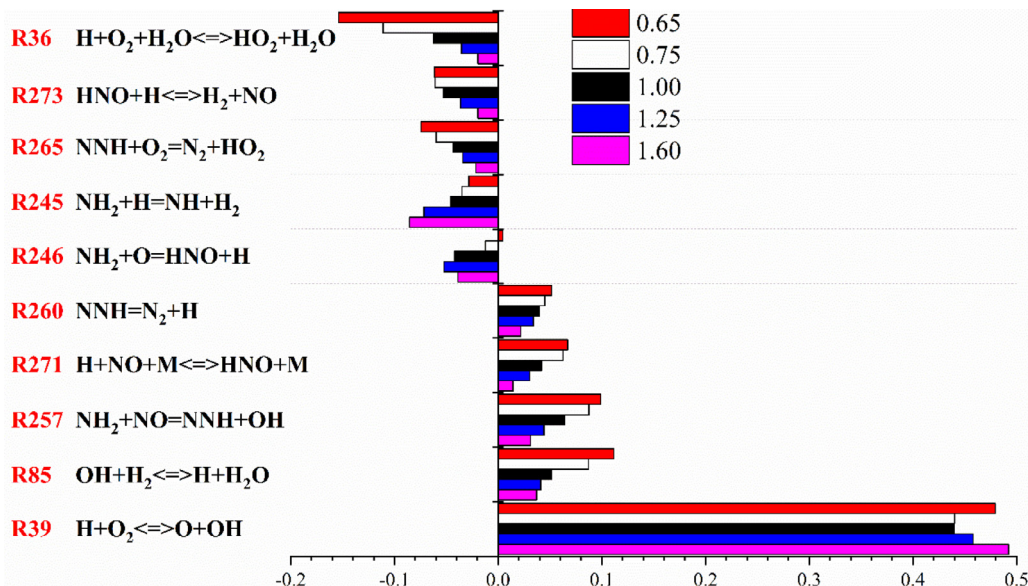


Fig. 6. Normalized sensitivity coefficients of the 10 most rate-limiting reactions on flame speeds in $NH_3/H_2/air$ ($X_{NH_3}/(X_{NH_3}+X_{H_2}) = 0.6$) flames for $\phi = 0.65, 0.75, 1.0, 1.25$ and 1.6 calculated using the Okafor et al. [12] mechanism.

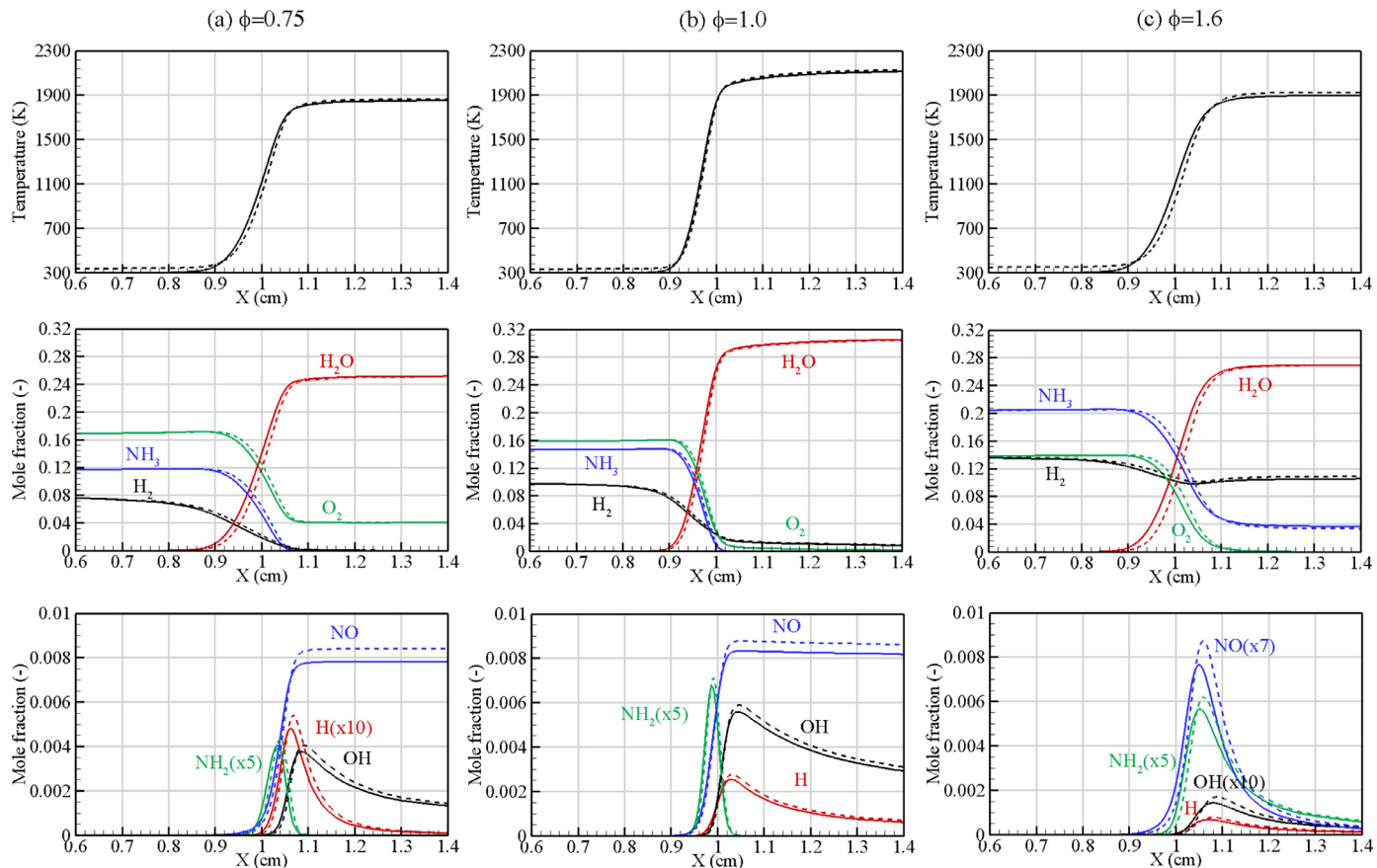


Fig. 7. Flame structures calculated by the ADI (solid) and SNB (dashed) models at $\phi = 0.75$ (a), 1.0 (b), and 1.6 (c).

ADI, due to the excessive estimations of the radiative heat loss and consequently more decreased temperatures in the burned region by the OTM (shown in Fig. 4). Whereas, the flame speeds calculated by the SNB were higher than those calculated by the ADI due to the radiation reabsorption. The increments of the flame speed in fuel-rich conditions were greater than those in fuel-lean conditions. Compared with the experimental data, the SNB exhibited

better predictions than the ADI and OTM, and agreed well with the measurements in the equivalence ratio range from 1.3 to 1.6. For the other equivalence ratios, the calculation results of all models were lower than the experimental data, whereas the SNB still provided closer predictions to the measured results. These discrepancies should be partially caused by the experimental uncertainties and the ammonia reaction mechanism of Okafor et al. [12].

Fig. 4 shows the distributions of the temperature and radiative power calculated by ADI, OTM and SNB at $\phi = 1.0$, to illustrate how the radiation reabsorption affected the flame speed. When the radiation reabsorption was considered, the thermal radiation of H_2O in the downstream high temperature zone was absorbed by NH_3 in the upstream low temperature zone, so that the radiative power of the unburned zone was negative and the unburned NH_3 was preheated, making the flame temperatures in the SNB higher than the ADI flame temperatures. On the other hand, when using SNB the radiation heat loss decreased in the downstream due to the radiation reabsorption of H_2O in the non-isothermal high temperature burned zone.

To quantify the effects of radiation reabsorption on laminar flame speeds at different equivalence ratios, the relative differences between ADI- and SNB-calculated flame speeds were expressed by $(S_{L, SNB} - S_{L, ADI}) / S_{L, ADI}$ and plotted in **Fig. 5(a)**. The results showed that the enhancement of flame speed by radiation reabsorption was nonlinearly dependent on equivalence ratio. There were two turning points separated the whole curve, resulting in a non-monotonic behavior. The relative difference, and hence the effect of radiation reabsorption, first increased when equivalence ratio was lower than 0.75, and then decreased with rising equivalence ratios in the range of 0.75–1.1, and finally increased again with increasing equivalence ratio. This behavior was caused by the combination of two coexisting effects, i.e., direct radiation effect and preheat-induced chemical effect. The direct radiation effect was dependent on the two factors, i.e., the absorption coefficient and the optical thickness [32]. As shown in **Fig. 5(b)**, when $NH_3:H_2$ ratio was fixed, the mole fraction of NH_3 increased with increasing equivalence ratio. Consequently, stronger radiation reabsorption occurred in the upstream due to the increased absorption coefficient of NH_3 . On the other hand, the optical thickness that blocked the radiation energy emitted by the burnt zone first decreased and then increased. Therefore, the enhancement of flame speed should always increase with increasing equivalence ratio when only considering the direct radiation effect.

Furthermore, the preheat-induced chemical effects on the enhancement of flame speed were examined. The sensitivities for flame speed of NH_3/H_2 /air flames with $X_{NH_3}/(X_{NH_3}+X_{H_2}) = 0.6$, and $\phi = 0.65, 0.75, 1.0, 1.25$ and 1.6 were analyzed using the Okafor et al. mechanism [12]. The top 10 reactions affecting the flame speed are shown in **Fig. 6**. The most positively sensitive reaction was R39 $H + O_2 \rightleftharpoons O + OH$ for all equivalence ratios. The most negatively sensitive reaction was R36 $H + O_2 + H_2O \rightleftharpoons HO_2 + H_2O$ for the lean cases and R245 $NH_2 + H \rightleftharpoons NH + H_2$ for the rich cases. Hence, it is clear that the H , OH and NH_2 radicals played important roles in the 10 most rate-limiting reactions.

Fig. 7 shows the streamwise profiles of temperature, major species (NH_3 , H_2 , O_2 and H_2O) and intermediate species (H , OH , NH_2 , NNH and NO) calculated by the ADI and SNB at $\phi = 0.75, 1.0$, and 1.6 . For the three equivalence ratios, the SNB flame temperatures were higher than the ADI flame temperatures, and the SNB unburned gas temperatures were also higher than the ADI unburned gas temperatures due to the radiation reabsorption. The mole fractions of major species predicted by SNB were similar to those by ADI. However, the mole fractions of intermediate species calculated by SNB were apparently greater than those by ADI. NH_2 was primarily produced through the reactions of NH_3 with OH and H , HNO was primarily formed through the reaction of NH_2 with O , and then oxidation of HNO mainly produced NO . Consequently, the increment of temperature facilitated these reactions and the mole fraction of NO was increased when radiation reabsorption was considered.

Since the H and OH radicals played key roles in the flame speeds under fuel-lean conditions, further examination was performed on the maximum mole fractions of H and OH at $\phi = 0.65$ – 1.0 .

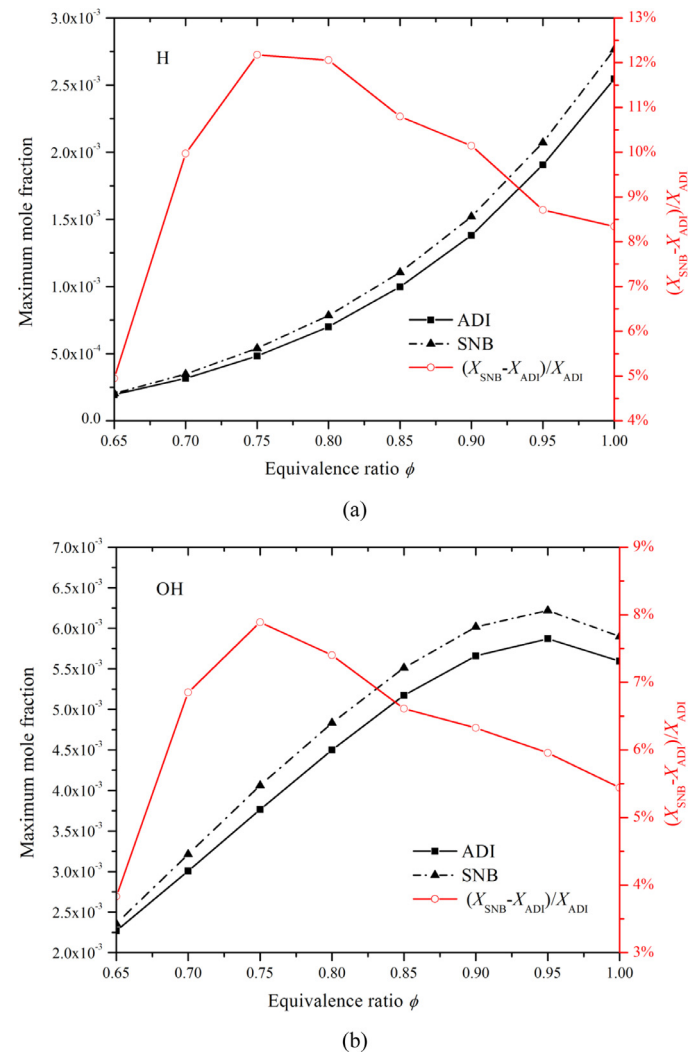


Fig. 8. Maximum mole fractions of the H (a) and OH (b) radicals calculated by the ADI (solid) and SNB (dashed) models for NH_3/H_2 /air flames at $\phi = 0.65-1.0$.

1.0. **Fig. 8** shows the effects of different radiation models, ADI and SNB, on the maximum mole fractions of the H and OH radicals at $\phi = 0.65-1.0$. For H radical, the relative increment of its maximum mole fractions increased from 4.95% to 12.2% with the equivalence ratio increasing from 0.65 to 0.75, which then decreased to 8.34% with further increasing equivalence ratios to 1.0. For OH radical, the relative increment of the maximum mole fractions increased from 3.83% to 7.89% with the equivalence ratio rising from 0.65 to 0.75, and then kept decreasing down to 5.44% with the equivalence ratio further enhanced to 1.0. Therefore, the change trends of radiation reabsorption effects on the maximum mole fractions of the H and OH radicals were similar to the radiation absorption effects on the laminar flame speed at $\phi = 0.65-1.0$ as discussed above and shown in **Fig. 5(a)**.

To better understand the chemical effects on the H and OH radicals mole fractions, **Fig. 9** presents the calculated rate of production (ROP) and normalized sensitivity coefficients of the 10 most important reactions on the H and OH radicals for NH_3/H_2 /air flames with $X_{NH_3}/(X_{NH_3}+X_{H_2}) = 0.6$, and $\phi = 0.65, 0.75$ and 1.0 on the current model. With increasing equivalence ratio, the absolute values of ROP for most reactions increased while the sensitivities decreased. In **Fig. 9(a1)**, among the reactions that consume H radicals, R39 $H + O_2 \rightleftharpoons O + OH$ and R36 $H + O_2 + H_2O \rightleftharpoons HO_2 + H_2O$ had the highest ROPs. As shown with the normalized sensitivi-

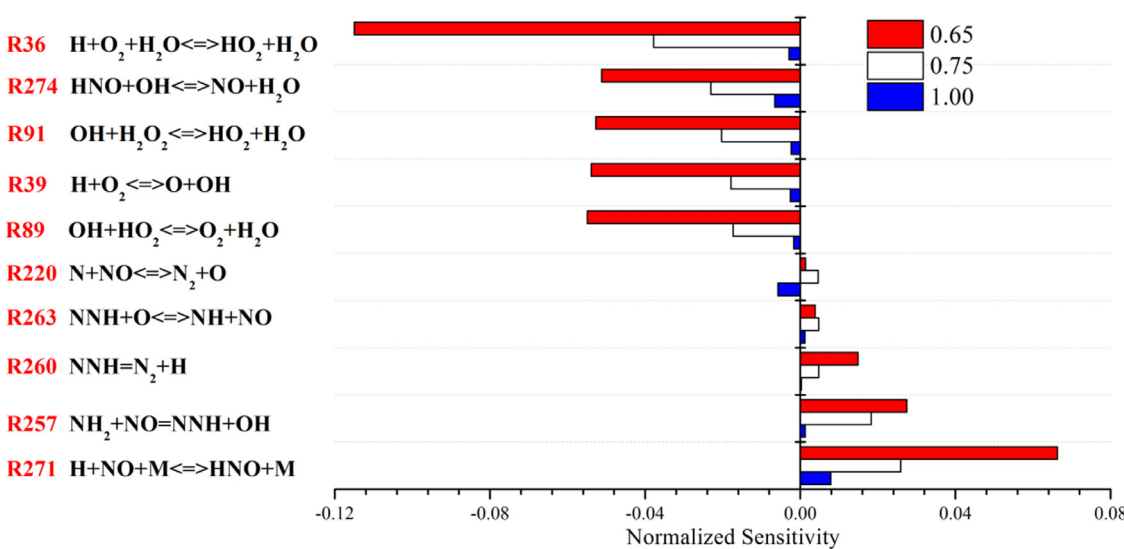
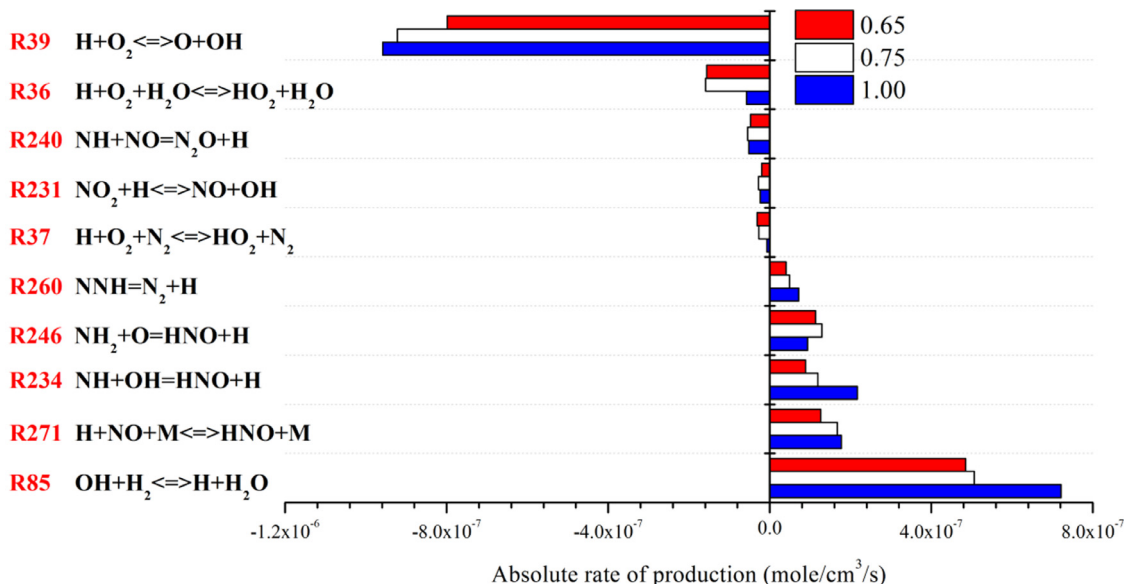


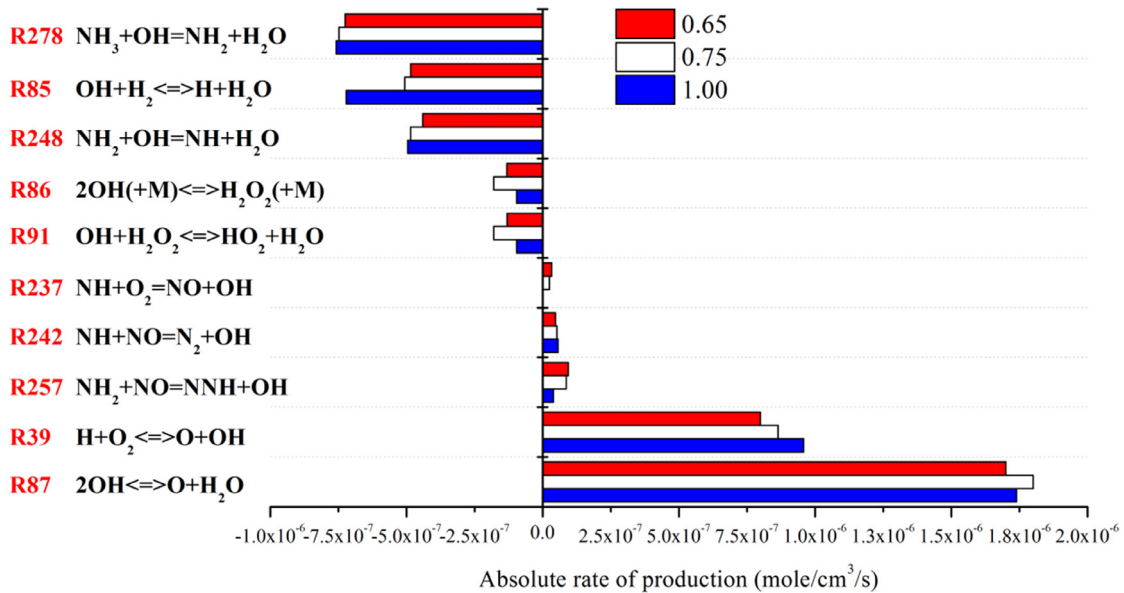
Fig. 9. ROP analysis results and normalized sensitivity coefficients of H (a1), (a2) and OH (b1), (b2) radicals for $\text{NH}_3/\text{H}_2/\text{air}$ flames ($X_{\text{NH}_3}/(X_{\text{NH}_3}+X_{\text{H}_2}) = 0.6$) at $\phi = 0.65, 0.75$ and 1.0 with the condition of $T_b = 300 \text{ K}$, $P = 1 \text{ atm}$.

ties for H radical concentrations in Fig. 9(a2), reaction R36 had the largest negative sensitivity for all equivalence ratios. Among the reactions that generate H radicals, R85 $\text{OH}+\text{H}_2 \rightleftharpoons \text{H} + \text{H}_2\text{O}$ and R234 $\text{NH}+\text{OH}=\text{HNO}+\text{H}$ had the highest ROPs, which however, were not among the top positive sensitivity reactions for H radical concentrations. Considering the top reactions affecting the flame speed in Fig. 6, it could be concluded that reaction R36 via H radical played the key role in the flame speed at $\phi = 0.65\text{--}1.0$.

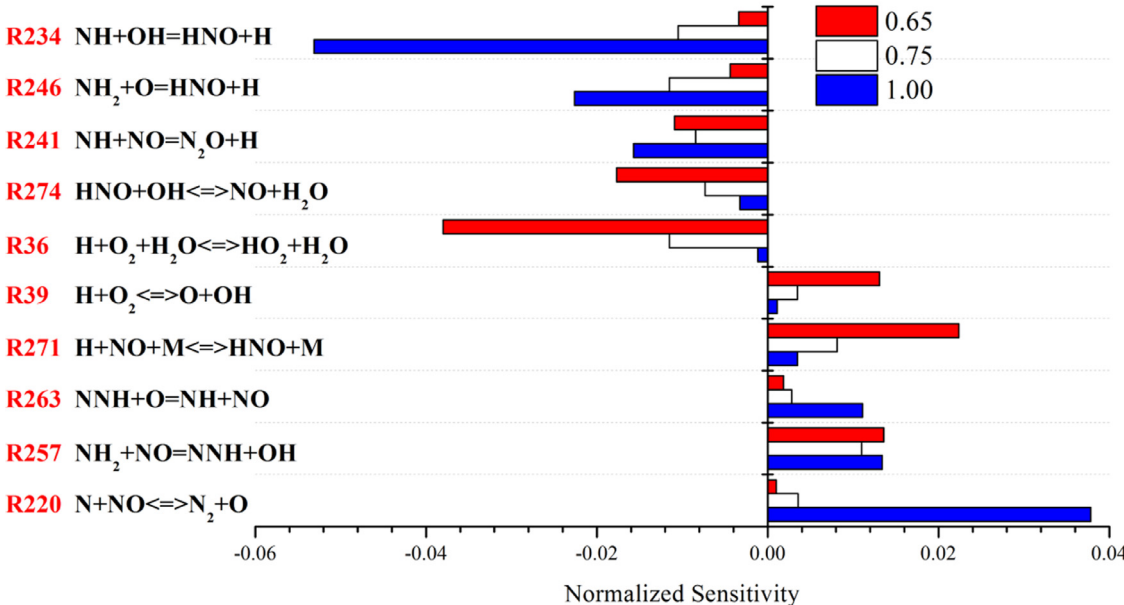
In Fig. 9(b1), among the reactions consuming OH radicals, R278 $\text{NH}_3+\text{OH}=\text{NH}_2+\text{H}_2\text{O}$, R85 $\text{OH}+\text{H}_2 \rightleftharpoons \text{H} + \text{H}_2\text{O}$ and R248 $\text{NH}_2+\text{OH}=\text{NH}+\text{H}_2\text{O}$ had the highest ROPs. However, these reactions were not among the top negatively sensitive reactions for OH radical concentrations. Among the reactions that generate OH radical, R39 $\text{H} + \text{O}_2 \rightleftharpoons \text{O}+\text{OH}$ and R257 $\text{NH}_2+\text{NO}=\text{NNH}+\text{OH}$ exhibited highest ROPs. As shown the normalized sensitivities for OH radical concentration in Fig. 9(b2), these two reactions were also

most significant for all equivalence ratios. In addition, reactions R39 and R257 were in the top reactions for the sensitivity of flame speed as shown in Fig. 6.

Since the temperature of the unburned zone increased through the radiation reabsorption, we next analyzed the effect of initial temperature change on the ROP results for R36 (H radical), R39 and R257 (OH radical) reactions at different equivalence ratios. As shown in Fig. 10(a), the ROP results decreased when the initial temperature increased except for R39 at $\phi=0.65$ and 0.7. The effect of initial temperature change on R39 was negligible since the absolute value of relative ROP differences were less than 1%. The consumption of H radicals by R36 was inhibited by increased initial temperature as evidenced by the decreased ROP. For this reason, the maximum mole fractions of the H radicals predicted by the SNB model were greater than those by the ADI as shown in Fig. 8(a). The absolute values of ROP relative differences of R36 in-



(b1)



(b2)

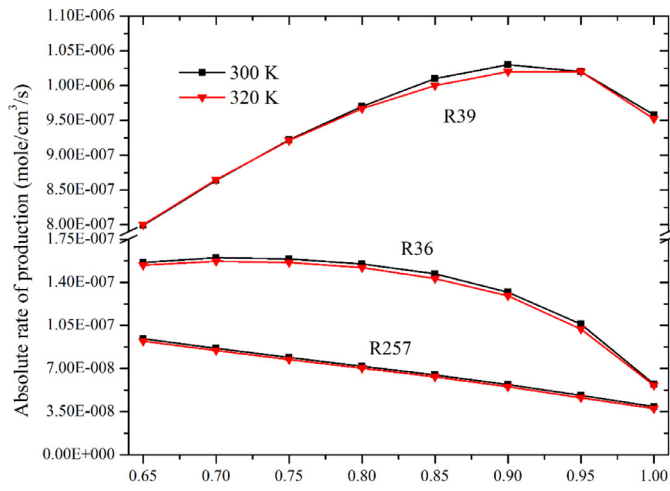
Fig. 9. Continued

creased at $\phi = 0.65\text{--}0.75$ (see Fig. 10(b)), indicating that the inhibition of the H consumption by R36 was progressively aggravated. Therefore, the maximum mole fractions of H radical increased at $\phi=0.65\text{--}0.75$ as shown in Fig. 8(a). On the other hand, R36 was the most negatively sensitive reaction for flame speed as evidenced in Fig. 6. The inhibition of R36 due to increased initial temperature caused the increment of flame speeds. Therefore, with the rising inhibition effect of R36, flame speeds were enhanced by radiation reabsorption at $\phi = 0.65\text{--}0.75$ (see Fig. 5(a)).

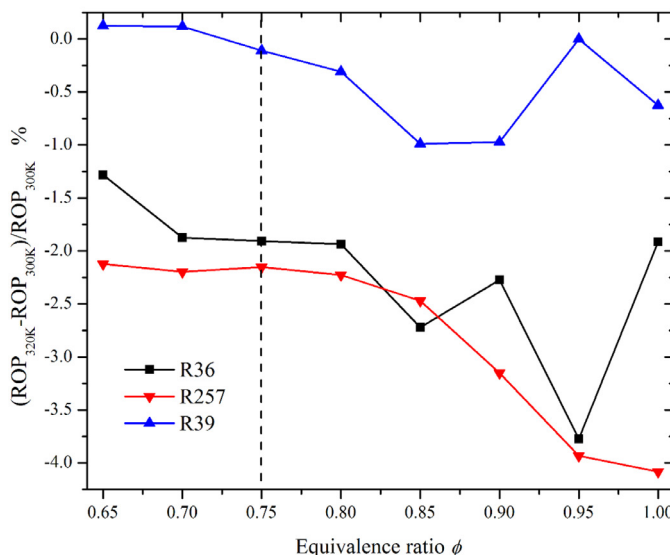
The generation of OH radicals by R257 was suppressed due to reduced initial temperature, as reflected by the ROP results. Hence, the maximum mole fractions of the OH radical predicted by the SNB model were greater than those by the ADI, as shown in Fig. 8(b). The absolute values of ROP relative differences for R257

increased at $\phi = 0.75\text{--}1.0$ (see Fig. 10(b)), which meant that the generation of OH radicals by R257 was progressively suppressed. Consequently, the relative increment of OH maximum mole fractions decreased at $\phi = 0.75\text{--}1.0$ (see Fig. 8(b)). Moreover, R257 was among the top 5 positively sensitive reactions for flame speed in Fig. 6. With the increasing inhibition effect of R257, the enhancement of flame speed by radiation reabsorption decreased at $\phi = 0.75\text{--}1.0$ as shown in Fig. 5(a).

Under fuel-rich conditions, investigation was conducted to reveal the effects of different radiation models, i.e., ADI and SNB, on the maximum mole fractions of the NH₂ radical at $\phi = 1.0\text{--}1.25$, which are plotted in Fig. 11. It can be seen the relative increment of the maximum mole fraction decreased from 5.66% to 4.99% as the equivalence ratio increased from 1.0 to 1.1, which then



(a)



(b)

Fig. 10. (a) ROP as a function of equivalence ratio for R36, R39 and R257 at two different initial temperatures 300 K and 320 K, and (b) relative differences of ROP for $\text{NH}_3/\text{H}_2/\text{air}$ flames at $\phi = 0.65\text{--}1.0$.

increased to 5.85% with the equivalence ratio increased to 1.25. Therefore, the non-monotonic effects of radiation reabsorption on the maximum mole fractions of the NH_2 radical were similar to the aforementioned radiation absorption effects on the laminar flame speed at $\phi = 1.0\text{--}1.25$ in Fig. 5(a).

In Fig. 12, among the reactions that consume NH_2 radicals, the reactions with highest ROPs were R245 $\text{NH}_2+\text{H}\rightleftharpoons\text{NH}+\text{H}_2$, R248 $\text{NH}_2+\text{OH}\rightleftharpoons\text{NH}+\text{H}_2\text{O}$ and R246 $\text{NH}_2+\text{O}\rightleftharpoons\text{HNO}+\text{H}$. As for the normalized sensitivities for NH_2 radical concentration, R248, R245 and R246 were the most negatively sensitive at all equivalence ratios. Among the reactions that generate NH_2 radicals, R278 $\text{NH}_3+\text{OH}\rightleftharpoons\text{NH}_2+\text{H}_2\text{O}$ and R277 $\text{NH}_3+\text{H}\rightleftharpoons\text{NH}_2+\text{H}$ had the highest ROPs. These two reactions were however not among the top positively sensitive reactions for NH_2 . On the other hand, R273 $\text{HNO}+\text{H}\rightleftharpoons\text{H}_2+\text{NO}$, R265 $\text{NNH}+\text{O}_2\rightleftharpoons\text{N}_2+\text{HO}_2$, R245 and R246 were the most negatively sensitive reactions on flame speed, which were all involved nitrogen element (see Fig. 6). Moreover, HNO in R273 was mainly generated through R246. Also considering the ROP results, as one of the most important reactions affecting NH_2

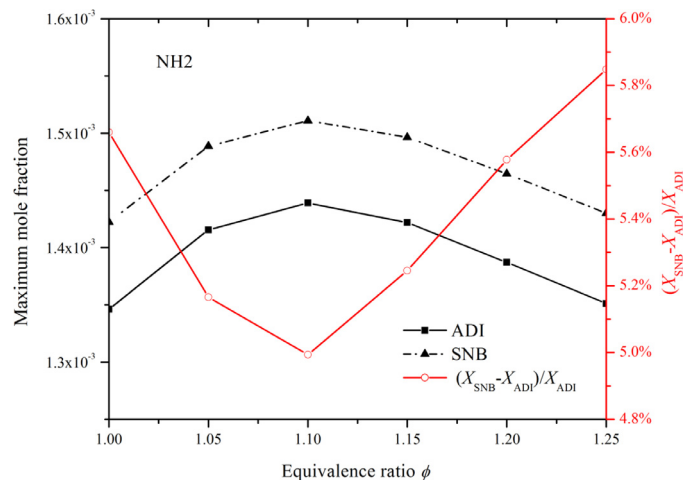


Fig. 11. Maximum mole fractions of the NH_2 radical predicted by the ADI (solid) and SNB (dashed) models for $\text{NH}_3/\text{H}_2/\text{air}$ flames at $\phi = 1.0\text{--}1.25$.

radical concentration, R246 through NH_2 radical played a key role in affecting the flame speeds at $\phi = 1.0\text{--}1.25$.

In addition, we analyzed the effects of initial temperature on the ROP results on R246. As shown in Fig. 13, the consumption of NH_2 radicals was prompted by R246 with increased initial temperature as reflected by the ROP results. Thus, the maximum mole fractions of the NH_2 radical predicted by the SNB model were greater than those by the ADI as shown in Fig. 11. The absolute values of ROP relative differences of R246 increased at $\phi = 1.0\text{--}1.1$, indicating that the enhancement of NH_2 consumption by R246 was constantly strengthening. Therefore, the relative increment of the maximum NH_2 mole fractions decreased at $\phi = 1.0\text{--}1.1$ as shown in Fig. 11. Subsequently, the absolute values of ROP relative differences of R246 decreased at $\phi = 1.1\text{--}1.25$, which meant that the promotion of NH_2 consumption via R246 was progressively weakening. Hence, the relative increment of NH_2 maximum mole fraction increased at $\phi = 1.1\text{--}1.25$ (see Fig. 11). Since R246's promoting effect increased first and then decreased in the range of $\phi = 1.00\text{--}1.25$, the enhancement of flame speed by radiation reabsorption decreased at $\phi = 1.0\text{--}1.1$ and increased at $\phi = 1.1\text{--}1.25$, as shown in Fig. 5(a). At even richer cases above $\phi=1.25$ in Fig. 5, the mole fraction of NH_3 increased with increasing equivalence ratio and hence the maximum optical thickness was less than that in the fuel-lean cases. The enhancement of flame speed became primarily controlled by the direct radiation effect.

3.2. Effects of pressure

In order to facilitate numerical convergence so as to assess a broader pressure range, in this section the $\text{NH}_3:(\text{NH}_3+\text{H}_2)$ ratio was reduced to 0.4, which nonetheless, did not alter the observed physics and conclusions. Laminar flame speeds as a function of pressure (up to 25 atm) calculated by the different radiation models, ADI, OTM and SNB, for stoichiometric $\text{NH}_3/\text{H}_2/\text{air}$ mixtures ($X_{\text{NH}_3}/(X_{\text{NH}_3}+X_{\text{H}_2}) = 0.4$) are shown in Fig. 14. Laminar flame speeds decreased with rising pressures in all the three models. The SNB simulations yielded higher results than those from the ADI model due to the radiation reabsorption. The effects of radiation reabsorption first increased quickly from 3.08% to 12.06% with the pressure increased to 10 atm, and then decreased to 10.16%. The effects of radiation reabsorption were the results of competition between the absorption coefficient and the optical thickness as shown in Fig. 15. The quantity $X_{\text{NH}_3}P$ was used to represent the radiation reabsorption from upstream since the absorption coefficient of NH_3 was directly proportional to $X_{\text{NH}_3}P$. Although $X_{\text{NH}_3}P$

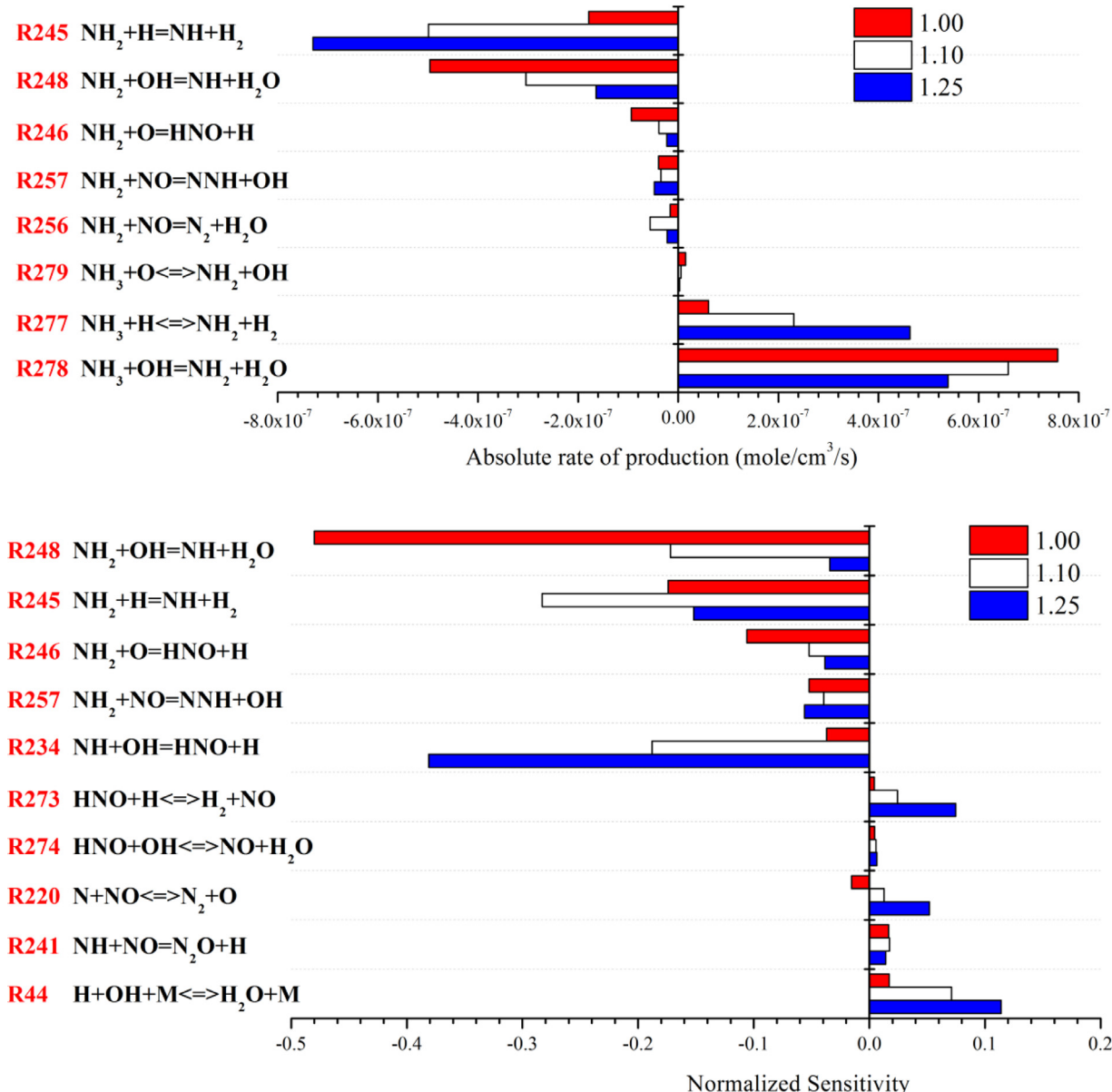


Fig. 12. ROP analysis results and normalized sensitivity coefficients of NH_2 radical for $\text{NH}_3/\text{H}_2/\text{air}$ flames ($X_{\text{NH}_3}/(X_{\text{NH}_3}+X_{\text{H}_2}) = 0.6$) at $\phi = 1.0, 1.1$ and 1.25 with the condition of $T_b = 300 \text{ K}$, $P = 1 \text{ atm}$.

increased with the pressure, the optical thickness increased more drastically from 0.035 to 0.8, which was 15 times larger than that in Fig. 5(b), indicating more thermal radiation energy was blocked at high pressures.

Subsequently, we examined the chemical effect on the enhancement of flame speed at $P = 1\text{--}10 \text{ atm}$. The sensitivities for flame speed of $\text{NH}_3/\text{H}_2/\text{air}$ flames with $X_{\text{NH}_3}/(X_{\text{NH}_3}+X_{\text{H}_2}) = 0.4$, $\phi = 1.0$ and $P = 1, 5, 10 \text{ atm}$ were analyzed using Okafor et al. mechanism [12]. The top 10 reactions affecting the flame speed are shown in Fig. 16. The most positively sensitive reaction was R39 $\text{H} + \text{O}_2 \rightleftharpoons \text{O} + \text{OH}$ and the most negatively sensitive reaction was R36 $\text{H} + \text{O}_2 + \text{H}_2\text{O} \rightleftharpoons \text{HO}_2 + \text{H}_2\text{O}$ at all pressures. It could be seen that the H , OH , NH_2 and NNH radicals played important roles in the 10 most rate-limiting reactions.

Fig. 17 shows the effects of different radiation models of ADI and SNB, on the maximum mole fractions of the H , OH , NH_2 and NNH radicals at $P = 1\text{--}10 \text{ atm}$. The relative increment of the maximum mole fractions of the four radicals increased with rising pres-

sure. The relative increments of the maximum mole fractions of H and NNH radicals were more severe than those of OH and NH_2 radicals. The non-monotonic effects of radiation reabsorption on the maximum mole fractions of the H and NNH radicals were similar to the radiation absorption effects on the laminar flame speed at $P = 1\text{--}10 \text{ atm}$ in Fig. 14.

To better understand the chemical effects on the H and NNH radicals, Fig. 18 shows the calculated rates of production (ROP) and sensitivities of the H and NNH radicals of the top 10 reactions in $\text{NH}_3/\text{H}_2/\text{air}$ flames with $X_{\text{NH}_3}/(X_{\text{NH}_3}+X_{\text{H}_2}) = 0.4$, $\phi = 1.0$ and $P = 1\text{--}10 \text{ atm}$ using the adopted SNB model. With rising pressure, the absolute values of ROP for all reactions increased. In Fig. 18(a1), among the reactions that consume H radicals, the reactions with the highest ROPs were R39, R44 $\text{H} + \text{OH} + \text{M} \rightleftharpoons \text{H}_2\text{O} + \text{M}$ and R36. As for the normalized sensitivity for H radical concentration in Fig. 18(a2), only R44 was significantly negatively sensitive for all pressures. Among the reactions that generate H radicals, the reactions with the highest ROPs were R85 $\text{OH} + \text{H}_2 \rightleftharpoons \text{H} + \text{H}_2\text{O}$ and

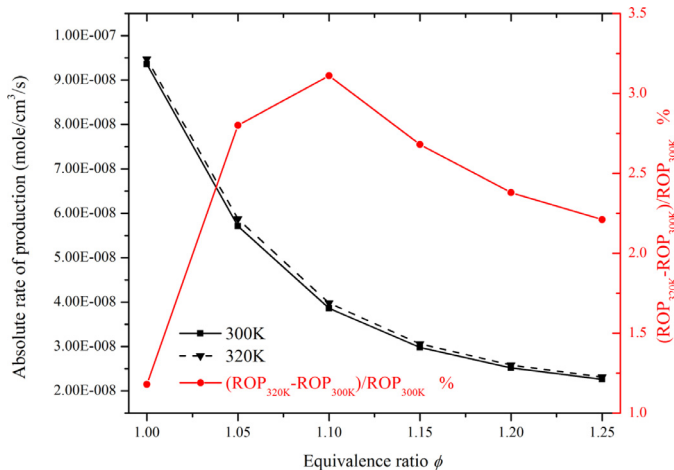


Fig. 13. ROP analysis results for R246 reaction at different initial temperatures 300 K and 320 K, and the corresponding ROP relative differences for NH₃/H₂/air flames at $\phi = 0.65\text{--}1.0$.

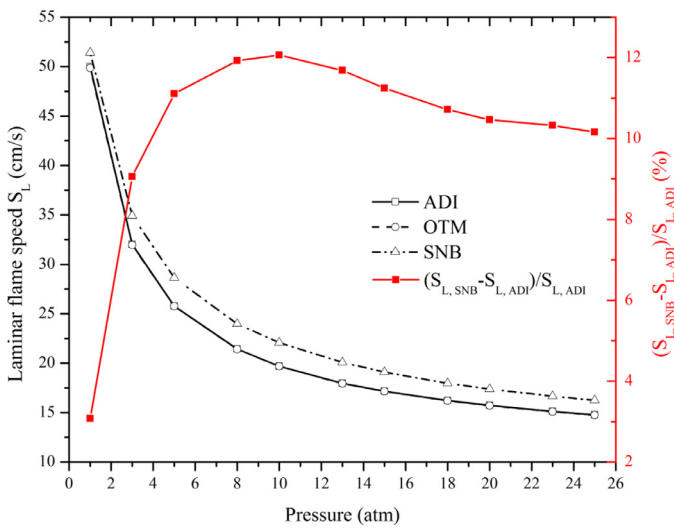


Fig. 14. Laminar flame speed calculated by different radiation models and radiation absorption effects on the laminar flame speed (relative difference between SNB and ADI results) as a function of pressure in planar NH₃/H₂/air ($X_{\text{NH}_3}/(X_{\text{NH}_3}+X_{\text{H}_2}) = 0.4$) flames at $\phi = 1.0$.

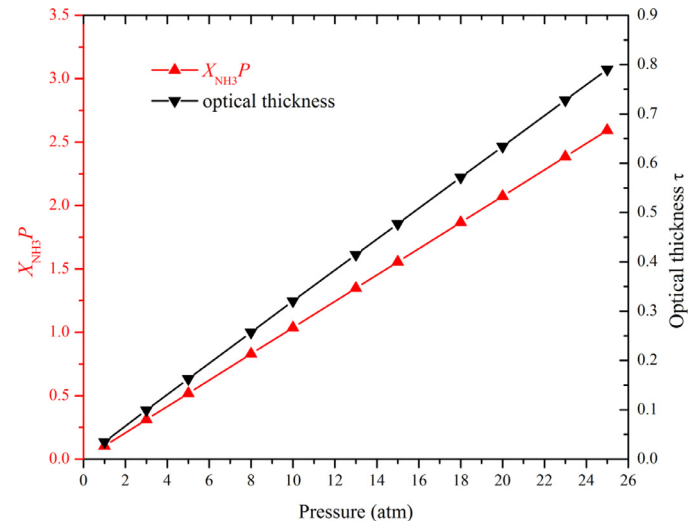


Fig. 15. $X_{\text{NH}_3}P$ in the upstream and optical thickness as a function of pressure in planar NH₃/H₂/air ($X_{\text{NH}_3}/(X_{\text{NH}_3}+X_{\text{H}_2}) = 0.4$) $\phi = 1.0$ flames.

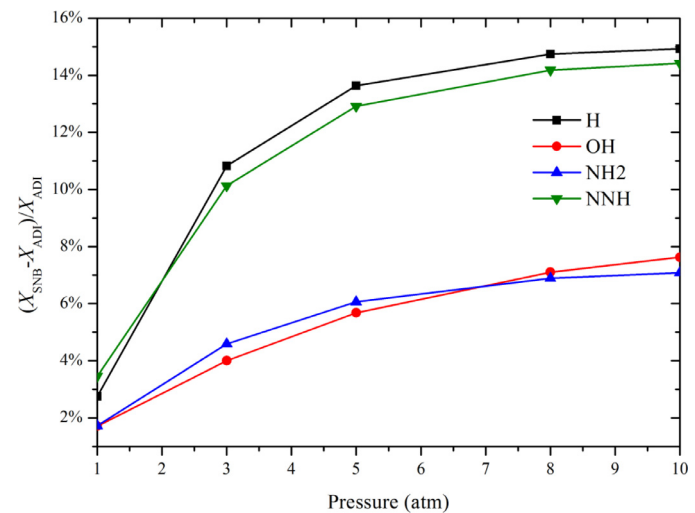


Fig. 17. Relative change of maximum mole fractions of the H, OH, NH₂ and NNH radicals computed using the ADI and SNB models for NH₃/H₂/air ($X_{\text{NH}_3}/(X_{\text{NH}_3}+X_{\text{H}_2}) = 0.4$) flames at $P = 1\text{--}10$ atm.

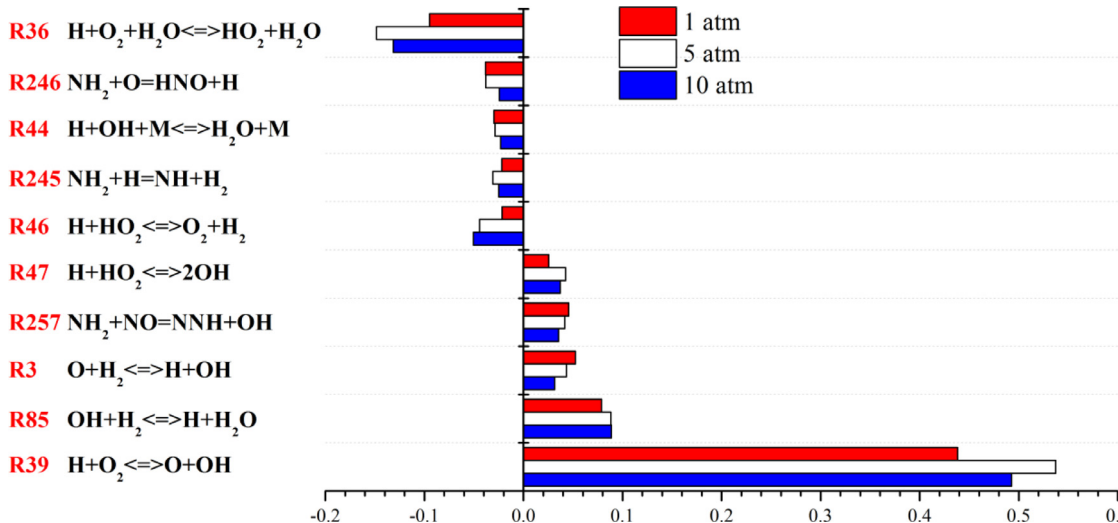
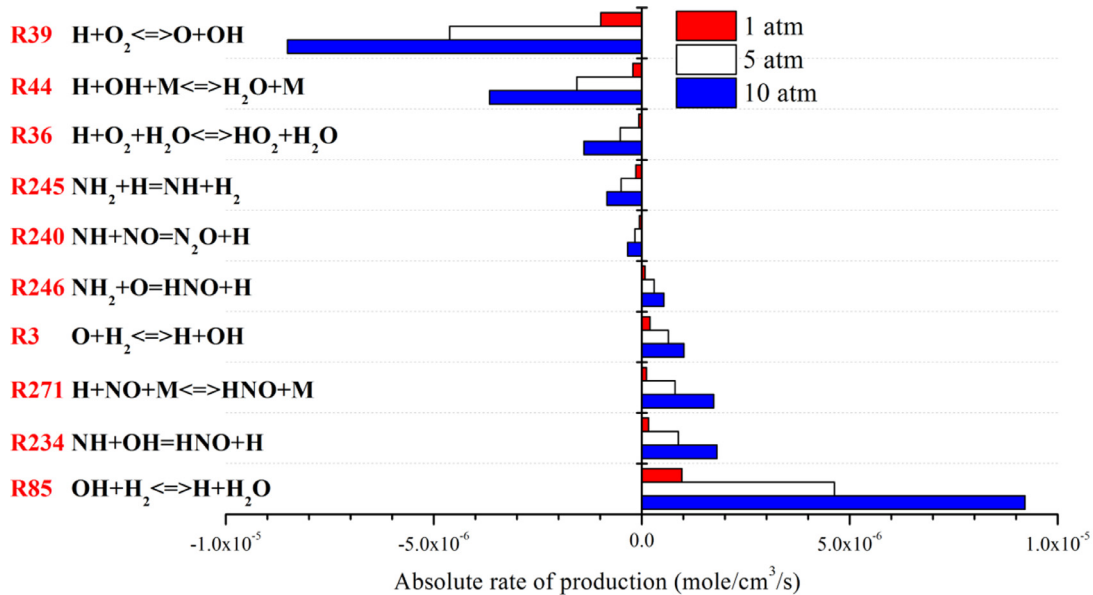
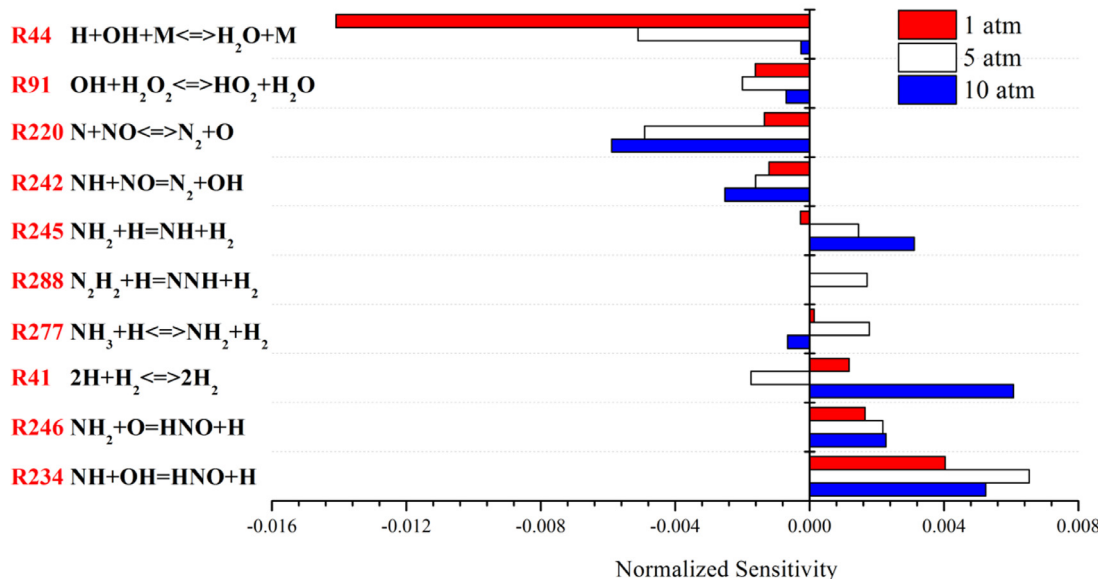


Fig. 16. Normalized sensitivity coefficients of flame speeds of the 10 most rate-limiting reactions in NH₃/H₂/air ($X_{\text{NH}_3}/(X_{\text{NH}_3}+X_{\text{H}_2}) = 0.4$) flames for $P = 1, 5, 10$ atm at $\phi = 1.0$.



(a1)



(a2)

Fig. 18. ROP results and normalized sensitivity coefficients of H (a1), (a2) and NNH (b1), (b2) radicals for $NH_3/H_2/\text{air}$ ($X_{NH_3}/(X_{NH_3}+X_{H_2}) = 0.4$) flames at $P = 1\text{--}10$ atm with the condition of $T_b = 300$ K, $\phi = 1.0$.

R234, and the latter was among the most positively sensitive reactions for H radical. Also considering the top reactions affecting the flame speed in Fig. 16, R44 (via H radical) played a key role in affecting the flame speed at pressures 1–10 atm.

In the Fig. 18(b1), for the consumption of NNH radicals, R260 $NNH + N_2 + H \rightleftharpoons NN + H_2$ and R265 $NNH + O_2 \rightleftharpoons N_2 + HO_2$ had the highest ROPs. However, these reactions were not included in the top negatively sensitive reactions for NNH in Fig. 18(b2). Among the reactions that generate NNH radicals, the reaction with the highest ROP was R257, which was also one of the top positively sensitive reactions for NNH radical concentration. Furthermore, R257 existed among the top reactions for the sensitivity of flame speed as shown in Fig. 16.

Finally, the effects of initial temperature change on the ROP results for R44 (H radical) and R257 (NNH radical) were analyzed at various pressures. As shown in Fig. 19, the ROP results decreased with the increasing initial temperature for both R44 and R257. The consumption of H radicals by R44 was inhibited as reflected by the decreased ROP of R44 with increased initial temperature. The maximum mole fractions of the H radicals by the SNB model were hence greater than those by the ADI shown in Fig. 17. As shown in Fig. 19(b), the absolute values of ROP relative differences for R44 increased at $P = 1\text{--}5$ atm, which meant that the inhibition of the H consumption by R36 was strengthened. Therefore, the relative increment of the maximum mole fractions of H radical increased at $P = 1\text{--}5$ atm as shown in Fig. 17. On the other hand, R44 was

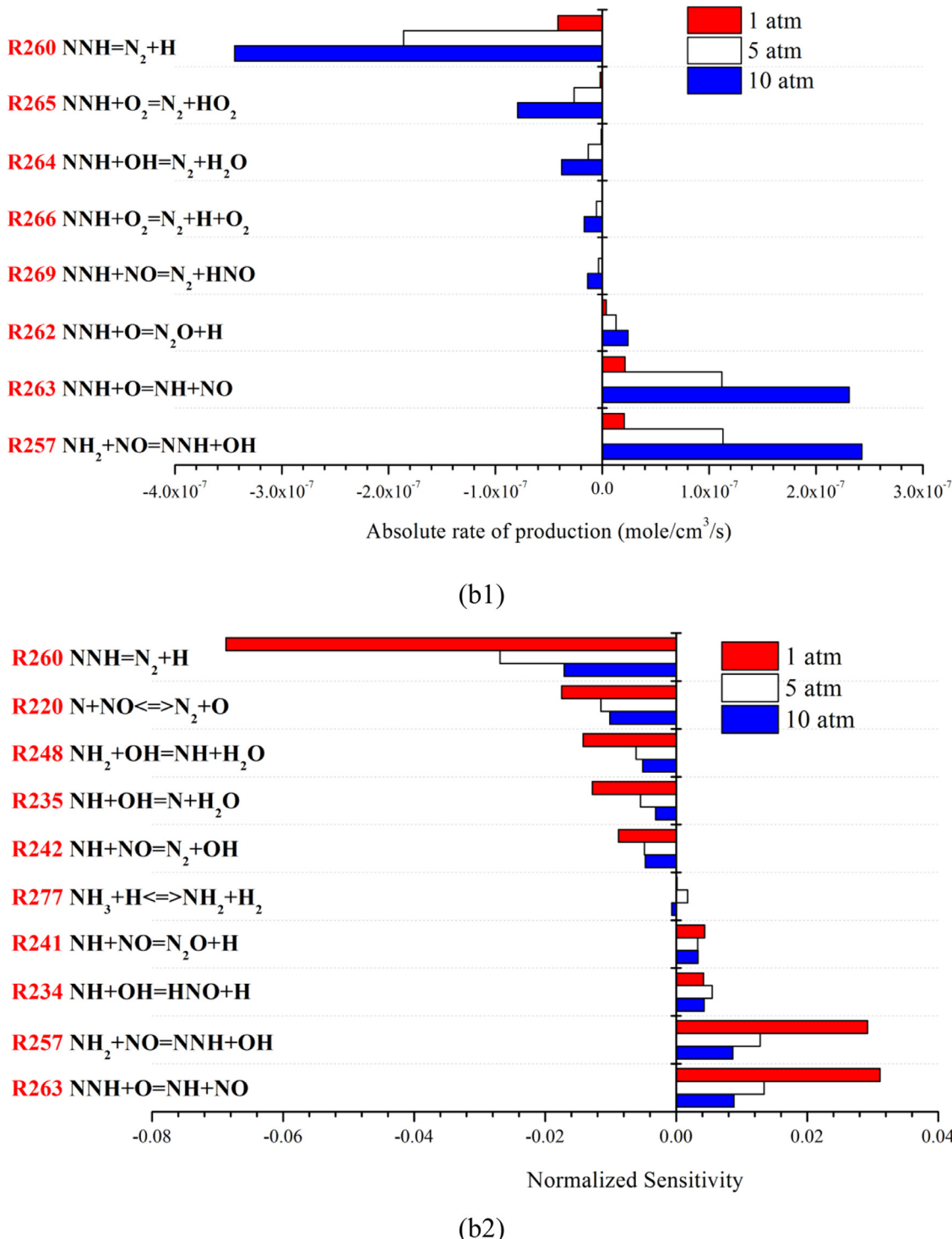


Fig. 18. Continued

the most negatively sensitive reaction for flame speed as shown in Fig. 16, and thus the inhibition of R44 due to higher initial temperature caused the increment of flame speed. Consequently, with the increasing inhibition effect of R44, the enhancement of flame speed by radiation reabsorption increased at $P = 1\text{--}5$ atm (see Fig. 14).

The generation of NNH radicals by R257 was inhibited (see the ROP results in Fig. 19(a)) by higher initial temperature, and hence the maximum mole fractions of the NNH radicals by the SNB were greater than those by the ADI (see Fig. 17). As shown in Fig. 19(b),

the absolute values of ROP relative differences of R257 decreased at $P = 5\text{--}10$ atm, indicating weakening suppression of NNH radicals by R257. Thus, the relative increment of the maximum mole fractions of NNH radicals increased at $P = 5\text{--}10$ atm as shown in Fig. 17. Moreover, R257 was among the top 5 positively sensitive reactions for flame speed in Fig. 16. With decreasing inhibition effect of R257, the enhancement of flame speed by radiation reabsorption increased at $P = 5\text{--}10$ atm (see Fig. 14). Above 10 atm as shown in Fig. 15, the radiation reabsorption effect decreased with increasing pressure due to the competition between the ab-

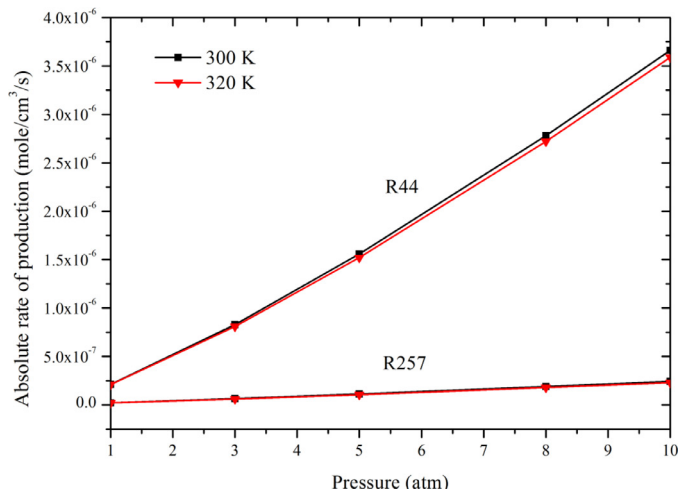


Fig. 19. (a) ROP analysis results for reactions R44 and R257 with different initial temperatures 300 K and 320 K, and (b) the ROP relative differences for NH₃/H₂/air (X_{NH₃}/(X_{NH₃}+X_{H₂}) = 0.4) flames at P = 1–10 atm.

sorption coefficient and optical thickness, and the optical thickness increased more with increasing pressure and the enhancement of flame speed was mainly controlled by the direct radiation effect.

4. Conclusions

Effects of radiation reabsorption on laminar flame speed of NH₃/H₂/air flames were investigated at $\phi = 0.65\text{--}1.6$, pressures 1–25 atm, NH₃:(NH₃+H₂) volumetric ratios 0.6 and 0.4. The SNB model for NH₃ was developed and applied for the computations of NH₃/H₂/Air flames radiation. The following conclusions can be drawn from this study.

- 1 Radiation reabsorption increased the flame speed and this enhancement effect exhibited a non-monotonic behavior for NH₃/H₂/air (NH₃:(NH₃+H₂) = 0.6) flames at $\phi = 0.65\text{--}1.6$. The maximum radiation reabsorption effect was up to 15.6%. Therefore, the radiation reabsorption needs to be included in quantitative predictions of flame speeds for ammonia flames.
- 2 The effects of radiation reabsorption were controlled by both direct radiation effect and preheat-induced chemical effect. At $\phi = 0.65\text{--}1.25$, the preheat-induced chemical effect dominated,

while the enhancement of flame speed by radiation reabsorption was mainly influenced by H, OH and NH₂ radicals, which were in turn controlled by the reactions R36, R257 and R246, respectively. At $\phi = 1.25\text{--}1.6$, the direct radiation effect dominated and the enhancement of flame speed was primarily affected by the increasing mole fraction of NH₃.

- 3 For stoichiometric NH₃/H₂/air (NH₃:(NH₃+H₂) = 0.4) flames at pressures 1–25 atm, the radiation reabsorption effect first increased and then decreased with rising pressures. At $P = 1\text{--}10$ atm, the preheat-induced chemical effect dominated and the enhancement of flame speed by radiation reabsorption was mainly determined by H and NNH radicals, which were controlled by the reactions R44 and R257, respectively. At high pressures above 10 atm, the direct radiation effect dominated and the enhancement of flame speed was mainly controlled by the increasing optical thickness.

Declaration of Competing Interest

The authors declare that they have no known competing financial interests or personal relationships that could have appeared to influence the work reported in this paper.

Acknowledgments

SZ acknowledges the National Key Research Development Program of China (No. 2017YFB0601900), the National Natural Science Foundation of China (No. 51976057, 51922040 and 51827808), the Fundamental Research Funds for the Central Universities (No. 2020JG005, 2020DF01), the Foundation of State Key Laboratory of Coal Combustion (No. FSKLCCA2104) and the Hunan Science and Technology Planning Project (2020RC5008). BZ acknowledges the Stable Support Plan Program of Shenzhen Natural Science Fund Grant (No. 20200925155430003).

References

- [1] A. Valera-Medina, H. Xiao, M. Owen-Jones, W.I.F. David, P.J. Bowen, Ammonia for power, *Prog Energy Combust Sci* 69 (2018) 63–102.
- [2] J.J. Mackenzie, W.H. Avery, Ammonia fuel: the key to hydrogen-based transportation, *Energy Conversion Engineering Conference, 1996. IECEC 96. Proceedings of the 31st Intersociety* (1996).
- [3] O. Kurata, N. Iki, T. Matsunuma, T. Inoue, T. Tsujimura, H. Furutani, H. Kobayashi, A. Hayakawa, Performances and emission characteristics of NH₃-air and NH₃/CH₄-air combustion gas-turbine power generations, *Proc. Combust. Inst.* 36 (2017) 3351–3359.
- [4] F.R. Westlye, A. Ivarsson, J. Schramm, Experimental investigation of nitrogen based emissions from an ammonia fueled SI-engine, *Fuel* 111 (2013) 239–247.
- [5] K. Takizawa, A. Takahashi, K. Tokuhashi, S. Kondo, A. Sekiya, Burning velocity measurements of nitrogen-containing compounds, *J. Hazard. Mater.* 155 (2008) 144–152.
- [6] F.J. Verkamp, M.C. Hardin, J.R. Williams, Ammonia combustion properties and performance in gas-turbine burners, *Symp. (Int.) Combust.* 11 (1967) 985–992.
- [7] A. Hayakawa, T. Goto, R. Mimoto, Y. Arakawa, T. Kudo, H. Kobayashi, Laminar burning velocity and Markstein length of ammonia/air premixed flames at various pressures, *Fuel* 159 (2015) 98–106.
- [8] P.D. Ronney, Effect of chemistry and transport properties on near-limit flames at microgravity, *Combust. Sci. Technol.* 59 (1988) 123–141.
- [9] A. Ichikawa, A. Hayakawa, Y. Kitagawa, K.D. Kunkuma Amila Somaratne, T. Kudo, H. Kobayashi, Laminar burning velocity and Markstein length of ammonia/hydrogen/air premixed flames at elevated pressures, *Int J Hydrogen Energy* 40 (2015) 9570–9578.
- [10] P. Kumar, T.R. Meyer, Experimental and modeling study of chemical-kinetics mechanisms for H₂-NH₃-air mixtures in laminar premixed jet flames, *Fuel* 108 (2013) 166–176.
- [11] X. Han, Z. Wang, M. Costa, Z. Sun, Y. He, K. Cen, Experimental and kinetic modeling study of laminar burning velocities of NH₃/air, NH₃/H₂/air, NH₃/CO/air and NH₃/CH₄/air premixed flames, *Combust. Flame* 206 (2019) 214–226.
- [12] E.C. Okafor, Y. Naito, S. Colson, A. Ichikawa, T. Kudo, A. Hayakawa, H. Kobayashi, Experimental and numerical study of the laminar burning velocity of CH₄-NH₃-air premixed flames, *Combust. Flame* 187 (2018) 185–198.
- [13] X. Han, Z. Wang, Y. He, Y. Zhu, K. Cen, Experimental and kinetic modeling study of laminar burning velocities of NH₃/syngas/air premixed flames, *Combust. Flame* 213 (2020) 1–13.

- [14] S. Wang, Z. Wang, A.M. Elbaz, X. Han, Y. He, M. Costa, A.A. Konnov, W.L. Roberts, Experimental study and kinetic analysis of the laminar burning velocity of NH₃/syngas/air, NH₃/CO/air and NH₃/H₂/air premixed flames at elevated pressures, Combust. Flame 221 (2020) 270–287.
- [15] A.J. Reiter, S.-C. Kong, Combustion and emissions characteristics of compression-ignition engine using dual ammonia-diesel fuel, Fuel 90 (2011) 87–97.
- [16] J.H. Lee, J.H. Kim, J.H. Park, O.C. Kwon, Studies on properties of laminar premixed hydrogen-added ammonia/air flames for hydrogen production, Int. J. Hydrogen Energy 35 (2010) 1054–1064.
- [17] S. Hansen, P. Glarborg, Simplified model for reburning chemistry, Energy Fuels 24 (2010) 4185–4192.
- [18] Z. Tian, Y. Li, L. Zhang, P. Glarborg, F. Qi, An experimental and kinetic modeling study of premixed NH₃/CH₄/O₂/Ar flames at low pressure, Combust. Flame 156 (2009) 1413–1426.
- [19] A.A. Konnov, Implementation of the NCN pathway of prompt-NO formation in the detailed reaction mechanism, Combust. Flame 156 (2009) 2093–2105.
- [20] U. Mechanism, Chemical-Kinetic Mechanisms for Combustion Applications, Mechanical and Aerospace Engineering (Combustion Research), University of California at San Diego, 2014.
- [21] E.C. Okafor, Y. Naito, S. Colson, A. Ichikawa, T. Kudo, A. Hayakawa, H. Kobayashi, Measurement and modelling of the laminar burning velocity of methane-ammonia-air flames at high pressures using a reduced reaction mechanism, Combust. Flame 204 (2019) 162–175.
- [22] K.P. Shrestha, L. Seidel, T. Zeuch, F. Mauss, Detailed kinetic mechanism for the oxidation of ammonia including the formation and reduction of nitrogen oxides, Energy Fuels 32 (2018) 10202–10217.
- [23] A. Stagni, C. Cavallotti, S. Arunthanayothin, Y. Song, O. Herbinet, F. Battin-Leclerc, T. Faravelli, An experimental, theoretical and kinetic-modeling study of the gas-phase oxidation of ammonia, React. Chem. Eng. 5 (2020) 696–711.
- [24] J.A. Miller, M.D. Smooke, R.M. Green, R.J. Kee, Kinetic modeling of the oxidation of ammonia in flames, Combust. Sci. Technol. 34 (1983) 149–176.
- [25] R.P. Lindstedt, F.C. Lockwood, M.A. Selim, Detailed kinetic modelling of chemistry and temperature effects on ammonia oxidation, Combust. Sci. Technol. 99 (1994) 253–276.
- [26] Ø. Skreiber, P. Kilpinen, P. Glarborg, Ammonia chemistry below 1400K under fuel-rich conditions in a flow reactor, Combust. Flame 136 (2004) 501–518.
- [27] Z. Tian, L. Zhang, Y. Li, T. Yuan, F. Qi, An experimental and kinetic modeling study of a premixed nitromethane flame at low pressure, Proc. Combust. Inst. 32 (2009) 311–318.
- [28] H. Nakamura, M. Shindo, Effects of radiation heat loss on laminar premixed ammonia/air flames, Proc. Combust. Inst. 37 (2019) 1741–1748.
- [29] Y. Ju, G. Masuya, P.D. Ronney, Effects of radiative emission and absorption on the propagation and extinction of premixed gas flames, Symp. (Int.) Combust. 27 (1998) 2619–2626.
- [30] Z. Chen, Effects of radiation and compression on propagating spherical flames of methane/air mixtures near the lean flammability limit, Combust. Flame 157 (2010) 2267–2276.
- [31] C.H. Sohn, Z. Chen, Y. Ju, Effects of radiation on the uncertainty of flame speed determination using spherically propagating flames with CO/CO₂/H₂O dilutions at elevated pressures, Int. J. Heat Mass Transf. 86 (2015) 820–825.
- [32] S. Zheng, R. Sui, W. Liang, H. Zhou, C.K. Law, On band lumping, radiation reabsorption, and high-pressure effects in laminar flame propagation, Combust. Flame 221 (2020) 86–93.
- [33] R.J. Kee, J.F. Grcar, M.D. Smooke, J.A. Miller, E. Meeks, PREMIX: a Fortran Program for Modeling Steady Laminar One-Dimensional Premixed Flames, 1985 Sandia National Laboratories Report.
- [34] C. Ludwig, W. Malkmus, J. Reardon, J. Thomson, R. Goulard, Handbook of Infrared Radiation From Combustion Gases, 3080, NASA Special Publication, 1973 NASA sp-3080.
- [35] A. Soufiani, J. Taine, High temperature gas radiative property parameters of statistical narrow-band model for H₂O, CO₂ and CO, and correlated-K model for H₂O and CO₂, Int. J. Heat Mass Transf. 40 (1997) 987–991.
- [36] I.E. Gordon, L.S. Rothman, C. Hill, R.V. Kochanov, Y. Tan, P.F. Bernath, M. Birk, V. Boudon, A. Campargue, K.V. Chance, B.J. Drouin, J.M. Flaud, R.R. Gamache, J.T. Hodges, D. Jacquemart, V.I. Perevalov, A. Perrin, K.P. Shine, M.A.H. Smith, J. Tennyson, G.C. Toon, H. Tran, V.G. Tyuterev, A. Barbe, A.G. Császár, V.M. Devi, T. Furtenbacher, J.J. Harrison, J.M. Hartmann, A. Jolly, T.J. Johnson, T. Karman, I. Kleiner, A.A. Kyuberis, J. Loos, O.M. Lyulin, S.T. Massie, S.N. Mikhailenko, N. Moazzen-Ahmadi, H.S.P. Müller, O.V. Naumenko, A.V. Nikitin, O.L. Polyansky, M. Rey, M. Rotger, S.W. Sharpe, K. Sung, E. Starikova, S.A. Tashkun, J.V. Auwera, G. Wagner, J. Wilzewski, P. Wcislo, S. Yu, E.J. Zak, The HITRAN2016 molecular spectroscopic database, J. Quant. Spectrosc. Radiat. Transf. 203 (2017) 3–69.
- [37] F. Liu, Ö.L. Gülder, G.J. Smallwood, Y. Ju, Non-grey gas radiative transfer analyses using the statistical narrow-band model, Int. J. Heat Mass Transf. 41 (1998) 2227–2236.
- [38] J.G. Marakis, Application of narrow and wide band models for radiative transfer in planar media, Int. J. Heat Mass Transf. 44 (2001) 131–142.
- [39] J. Li, H. Huang, N. Kobayashi, Z. He, Y. Nagai, Study on using hydrogen and ammonia as fuels: combustion characteristics and NOx formation, Int. J. Energy Res. 38 (2014) 1214–1223.